

Circular band formation for incompressible viscous fluid–rigid-particle mixtures in a rotating cylinder

Suchung Hou,¹ Tsorng-Whay Pan,^{2,*} and Roland Glowinski²

¹*Department of Mathematics, National Cheng Kung University, Tainan 701, Taiwan, Republic of China*

²*Department of Mathematics, University of Houston, Houston, Texas 77204, USA*

(Received 13 March 2013; published 25 February 2014)

In this paper we have investigated a circular band formation of fluid–rigid-particle mixtures in a fully filled cylinder horizontally rotating about its cylinder axis by direct numerical simulation. These phenomena are modeled by the Navier-Stokes equations coupled to the Euler-Newton equations describing the rigid solid motion of the non-neutrally particles. The formation of circular bands studied in this paper is mainly caused by the interaction between particles themselves. Within a circular band, the part of the band formed by the particles moving from the front to the back through the upper portion of the cylinder becomes more compact due to the particle interaction strengthened by the speedup of the particle speeds first by the rotation and later by the rotation and the gravity. The part of a band formed by the particles moving from the back to the front through the lower portion of the cylinder is always loosening up and spreading out due to the slowdown of the particle motion first by the rotation and then by the rotation and the counter effect of the gravity. To have a compact circular band, particles have to interact among themselves continuously through the entire circular band at an angular speed so that the separation of particles can be balanced by their aggregation.

DOI: [10.1103/PhysRevE.89.023013](https://doi.org/10.1103/PhysRevE.89.023013)

PACS number(s): 47.54.–r, 47.11.–j, 47.55.Lm

I. INTRODUCTION

Nonequilibrium systems often organize into interesting spatiotemporal structures or patterns. Examples include the patterns in pure fluid flow systems, such as the Taylor-Couette flow between two concentric rotating cylinders and well-defined periodic bands of particles in a partially or fully filled horizontally rotating cylinder. Particulate flows exhibiting circular bands in a partially filled horizontal rotating cylinder are in part attributed to the presence of the free surface caused by the partial filling of the cylinder (e.g., see [1–3]). In a fully filled horizontally rotating cylinder, band and other pattern formations were also found in the suspensions of non-Brownian settling particles in [4–10]. For probably the most complete overview of the literature on the pattern formation and segregation in rotating-drum flows, please see the recent extensive review article by Seiden and Thomas [11]. Lee and Ladd [12,13] addressed the experimental observations made by Matson *et al.* [4–6] in creeping flow regime. The ratio of the particle diameter and the inner cylinder diameter in [4–6,12,13] is about 1%. In [12,13], numerical simulations within the Stokes-flow approximation have been used to investigate the mechanism underlying circular cluster formation. The numerical results show that the formation of the circular cluster is correlated with an inhomogeneous particle distribution in the radial plane, which is itself driven by the competition between the gravity and the viscous drag. The circular cluster structure develops during the transition between a low-frequency segregated phase and a high-frequency dispersed phase. In this paper, we have focused on the understanding of the band formation which looks like those observed in [9,10], but the values of the Reynolds number, $Re = 2aU/\nu$, and Ekman number, $E = \nu/\Omega R^2$, for the cases considered here are in a different regime, where a is

the ball radius, the characteristic velocity U is given by ΩR with the cylinder angular speed Ω and the cylinder radius R , and ν is the kinematic viscosity. Thus the numerical simulation is, strictly speaking, not comparable with the experiments [9,10]. The fluid-particle mixtures considered here are not in the creeping flow regime as considered computationally by Lee and Ladd in [12,13]. In [8], Lipson used a horizontal rotating cylinder filled with oversaturated solution to grow crystal without any interaction with a substrate and found that crystals accumulate in well-defined periodic bands, normal to the axis of rotation. Lipson and Seiden [9] just suggested, with no further discussion, that it could be the interaction between particles and fluid in the tube. In [10], Seiden *et al.* did an experimental investigation of the dependence of the formation of bands on particle characteristics, tube diameter and length, and fluid viscosity. They suggested that the segregation of particles occurs as a result of mutual interaction between the particles and inertial waves excited in the bounded fluid. In [14] Seiden *et al.* believed that the axial pressure gradient associated with an inertial-mode excitation within bounded fluid is responsible for the formation of bands according to their general dimensionless analysis. A single ball motion was discussed by solving the equation of motion for the ball with a one-way coupling in a filled and horizontally rotating cylinder; a stability analysis and a phase diagram based on one ball motion are addressed, but they did not consider the effect of the ball to the fluid and the interaction between particles themselves.

Via direct numerical simulations, we have observed that, for the cases considered in this paper, the formation of circular bands is mainly caused by the interaction between particles themselves. In our simulations, the particles form a layer inside a horizontally rotating cylinder similar to the one in Fig. 7 in [10]. These particles are partially coated on the inner wall of the rotating cylinder under the influence of a strong centrifugal force. Within a circular band, the part of the band formed by the particles moving from the front to the back through the upper portion of the cylinder becomes more compact due to the

*Corresponding author: pan@math.uh.edu

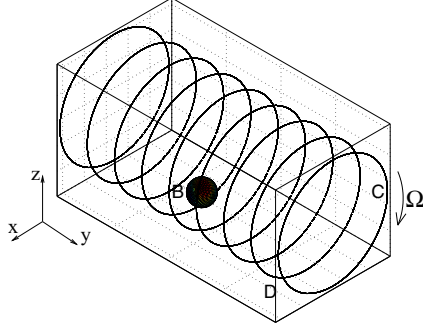


FIG. 1. (Color online) The flow region with a ball B in a truncated cylinder C .

particle interaction strengthened by the speedup of the particle speeds first by the rotation and then later by the rotation and the gravity. The part of a band formed by the particles moving from the back to the front through the lower portion of the cylinder is always loosening up and spreading out due to the slowdown of the particle motion first by the rotation and then by the rotation and the counter effect of the gravity. To have a compact circular band, particles have to interact among themselves continuously through the entire circular band at an angular speed so that the separation of particles can be balanced by their aggregation. Hence the balance of the gravity, the angular speed, and the fluid flow inertia and the number of particles is important to the formation of circular bands in a fully filled cylinder.

The scheme of this paper is as follows: We discuss the models and numerical methods briefly in Sec. II. In Sec. III, we study the effect of the particle number, the angular speed, and the initial gap size on the formation of circular bands and then present the flow field development under the influence of the particle interaction. The conclusions are summarized in Sec. IV.

II. MODEL AND NUMERICAL METHOD

To perform the direct numerical simulation of the interaction between rigid bodies and fluid, we have developed a methodology which combines a distributed Lagrange multiplier based fictitious domain method with operator splitting and finite element methods (e.g., see [15–20]). For a ball B moving in a Newtonian viscous incompressible fluid of the viscosity μ and the density ρ contained in a truncated cylinder C under the effect of the gravity depicted in Fig. 1, the flow is modeled by the Navier-Stokes equations, namely,

$$\rho \left[\frac{\partial \mathbf{u}}{\partial t} + (\mathbf{u} \cdot \nabla) \mathbf{u} \right] - \mu \Delta \mathbf{u} + \nabla p = \mathbf{g} \quad \text{in } \{(\mathbf{x}, t) | \mathbf{x} \in C \setminus \overline{B(t)}, t \in (0, T)\}, \quad (1)$$

$$\nabla \cdot \mathbf{u}(t) = 0 \quad \text{in } \{(\mathbf{x}, t) | \mathbf{x} \in C \setminus \overline{B(t)}, t \in (0, T)\}, \quad (2)$$

$$\mathbf{u}(0) = \mathbf{u}_0(\mathbf{x}) \quad (\text{with } \nabla \cdot \mathbf{u}_0 = 0), \quad (3)$$

$$\mathbf{u} = \mathbf{g}_0 \quad \text{on } \Gamma_0 \times (0, T) \quad \left(\text{with } \int_{\Gamma_0} \mathbf{g}_0 \cdot \mathbf{n} d\Gamma = 0 \right), \quad (4)$$

where Γ_0 is the entire surface of a truncated cylinder C , \mathbf{g} denotes gravity, \mathbf{g}_0 is the given velocity field, $\mathbf{u}_0(\mathbf{x})$ is the initial condition of flow field, and \mathbf{n} is the unit normal vector pointing outward to the flow region. We assume a *no-slip condition* on $\gamma (= \partial B)$. The motion of the rigid body B satisfies the Euler-Newton's equations, namely

$$\mathbf{v}(\mathbf{x}, t) = \mathbf{V}(t) + \boldsymbol{\omega}(t) \times \mathbf{G}(t)\mathbf{x}, \quad \forall \mathbf{x} \in \overline{B(t)}, \quad \forall t \in (0, T), \quad (5)$$

$$\frac{d\mathbf{G}}{dt} = \mathbf{V}, \quad (6)$$

$$M_p \frac{d\mathbf{V}}{dt} = M_p \mathbf{g} + \mathbf{F}_H, \quad (7)$$

$$\mathbf{I}_p \frac{d\boldsymbol{\omega}}{dt} = \mathbf{T}_H, \quad (8)$$

with the resultant and torque of the hydrodynamical forces given by, respectively,

$$\mathbf{F}_H = - \int_{\gamma} \boldsymbol{\sigma} \mathbf{n} d\gamma, \quad \mathbf{T}_H = - \int_{\gamma} \mathbf{G}\mathbf{x} \times \boldsymbol{\sigma} \mathbf{n} d\gamma \quad (9)$$

with $\boldsymbol{\sigma} = \mu(\nabla \mathbf{u} + \nabla \mathbf{u}^t) - p\mathbf{I}$. Equations (1)–(9) are completed by the following initial conditions:

$$\mathbf{G}(0) = \mathbf{G}_0, \quad \mathbf{V}(0) = \mathbf{V}_0, \quad \boldsymbol{\omega}(0) = \boldsymbol{\omega}_0, \quad B(0) = B_0. \quad (10)$$

Above, M_p , \mathbf{I}_p , \mathbf{G} , \mathbf{V} , and $\boldsymbol{\omega}$ are the mass, inertia, center of mass, velocity of the center of mass, and angular velocity of the rigid body B , respectively. The gravity is pointed downward in the direction of z .

To solve numerically the coupled problem (1)–(10), we have first applied a distributed Lagrange multiplier-based fictitious domain method (see [15] and [16] for details). Its basic idea is to imagine that the fluid fills the space inside as well as outside the particle boundaries. The fluid flow problem is then posed on a larger domain \mathbf{D} , the “fictitious domain.” The fictitious domain has a simple shape, allowing a simple regular mesh to be used. This domain is also time independent, so the same mesh can be used for the entire simulation. This is a great advantage, since for simulating three-dimensional (3D) interaction of fluid and particles, the automatic generation of unstructured boundary-fitted meshes for a large number of closely spaced particles considered in this paper is a difficult problem. The fluid inside the particle boundary must exhibit a rigid body motion of the particle. This constraint is enforced using a distributed Lagrange multiplier, which represents the additional body force per unit volume needed to maintain the rigid body motion inside the particle boundary, much like the pressure in incompressible fluid flow, whose gradient is the force required to maintain the constraint of incompressibility. The numerical scheme for solving the distributed Lagrange multiplier-based fictitious domain formulation of problem (1)–(10) has been fully discussed in [20]. For space discretization, we have used P_1 -iso- P_2 and P_1 finite elements for the velocity field and pressure, respectively (e.g., see [17,20]). In time advancing, via the Lie's scheme [21] with the finite element approximation, the fictitious domain formulation of problem (1)–(10) is decoupled into a sequence of simpler subproblems at each time step and solved numerically.

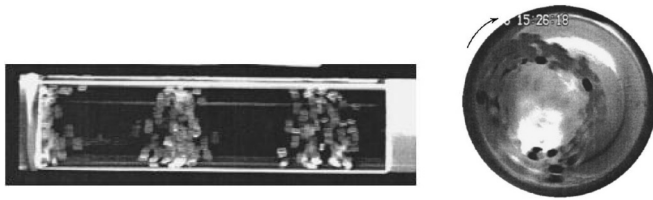


FIG. 2. Experimental photos from Ref. [10] with authors' permission.

III. NUMERICAL EXPERIMENTS AND DISCUSSION

A. Combined effect of the angular speed and the number of particles

To investigate the circular band formation for the suspensions of particles in a fully filled horizontally rotating cylinder, we have studied first the formation of a single circular band via the cases of 16, 24, 32, and 64 balls of radius $a = 0.075$ cm and density $\rho_p = 1.25$ g/cm³ in a truncated cylinder of diameter $2R = 1$ cm and length 4 cm filled with a fluid of the density 1 g/cm³ and kinematic viscosity $\nu = 0.15$ cm²/sec. The solid fractions are 0.9%, 1.35%, 1.8%, and 2.7%, respectively, for the cases of 16, 24, 32, and 64 balls. The initial positions of the ball mass centers are on the circles of radius 0.35 cm centered at the cylinder central axis with eight balls in each circle (see Figs. 3–6). We have perturbed each mass center randomly in the direction of the cylinder axis to break the symmetry of the initial pattern. The distance between two neighboring circles is about $2.25a$ hence the initial gap size d_g between balls in the cylinder axis direction is about $a/4$. In the simulations, the cylinder rotates about the cylinder axis parallel

to the y axis in a clockwise direction with angular speed Ω of either 8 or 12 rad/sec (see Fig. 1). The Reynolds numbers, $Re = 2aU/\nu$, with the characteristic velocity $U = \Omega R$ are 4 and 6, respectively, for $\Omega = 8$ and 12 rad/sec. The Reynolds numbers of the cases considered here are about two orders less than those considered in [10]. The Ekman numbers, $E = \nu/\Omega R^2$, are 0.075 and 0.05, respectively, for $\Omega = 8$ and 12 rad/sec and both are an order larger than those considered in [10]. Both numbers for the cases considered here are in a different regime, thus the numerical simulation is, strictly speaking, not comparable with the experiments [9,10] even though the circular band formation is similar to those observed in [9,10] (e.g., see Fig. 2). Since the thickness of the Ekman boundary layer is the order of $E^{1/2}$, our meshes can resolve the Ekman boundary layer for the cases studied in this paper.

The histories of the y coordinate of the particle mass centers and the positions of 16 balls at $t = 40$ sec obtained with the angular speed $\Omega = 8$ and 12 rad/sec in Figs. 3 and 7 clearly show that the 16 balls spread out in the cylinder axis direction and do not form a circular band at all. For the cases of 24 balls, the formation of the circular band is still not clear yet. In Figs. 4 and 7, the 24 balls spread out in the cylinder axis direction at the angular speed $\Omega = 8$ rad/sec. When the angular speed is 12 rad/sec, the 24 balls do form a loose circular band. For the cases of 32 balls, the formation of the circular band is clearly shown in Figs. 5 and 7. The one obtained at the angular speed $\Omega = 12$ rad/sec is very compact. For the cases of 64 balls, they split into two loose circular bands at $\Omega = 8$ rad/sec since it is not fast enough to produce strong particle interaction to sustain the whole group of particles as shown in Figs. 6 and 7. But at the angular speed $\Omega = 12$ rad/sec, there is just one compact circular band in which the particles are well organized in the

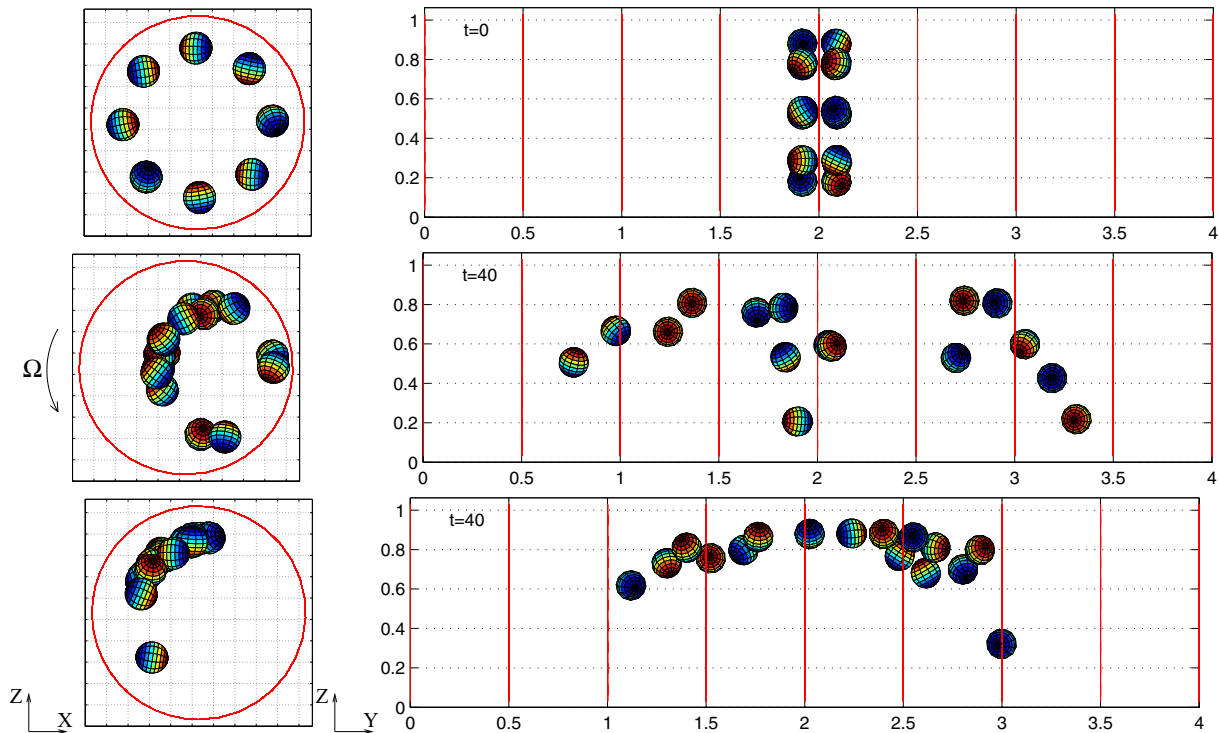


FIG. 3. (Color online) The side view (left) and the front view (right) of the initial position of 16 balls (top) and the position obtained at the angular speed $\Omega = 8$ (middle) and 12 (bottom) rad/sec at $t = 40$ sec.

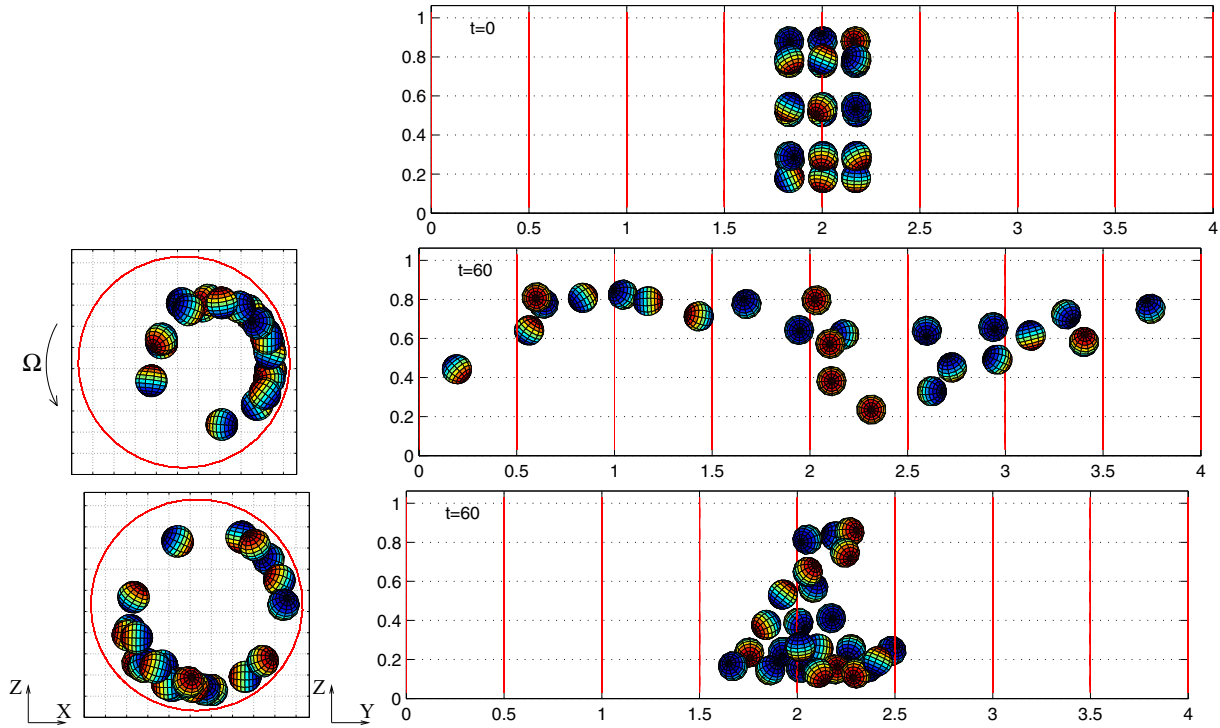


FIG. 4. (Color online) The side view (left) and the front view (right) of the initial position of 24 balls (top) and the position obtained at the angular speed $\Omega = 8$ (middle) and 12 (bottom) rad/sec at $t = 60$ sec.

middle due to the pushing from the outer balls. The particles form a layer inside the cylinder which is different from those observed in [4–6], but close to those in [9,10] (e.g, see Fig. 2). These results give us a simple observation which is that there is

a need of enough particles so that the particles within a circular band can continuously interact among themselves. For the case of 64 balls shown in Fig. 6 (respectively, Fig. 14), there are 33 and 31 balls (respectively, 29 and 35 in Fig. 14) in two bands,

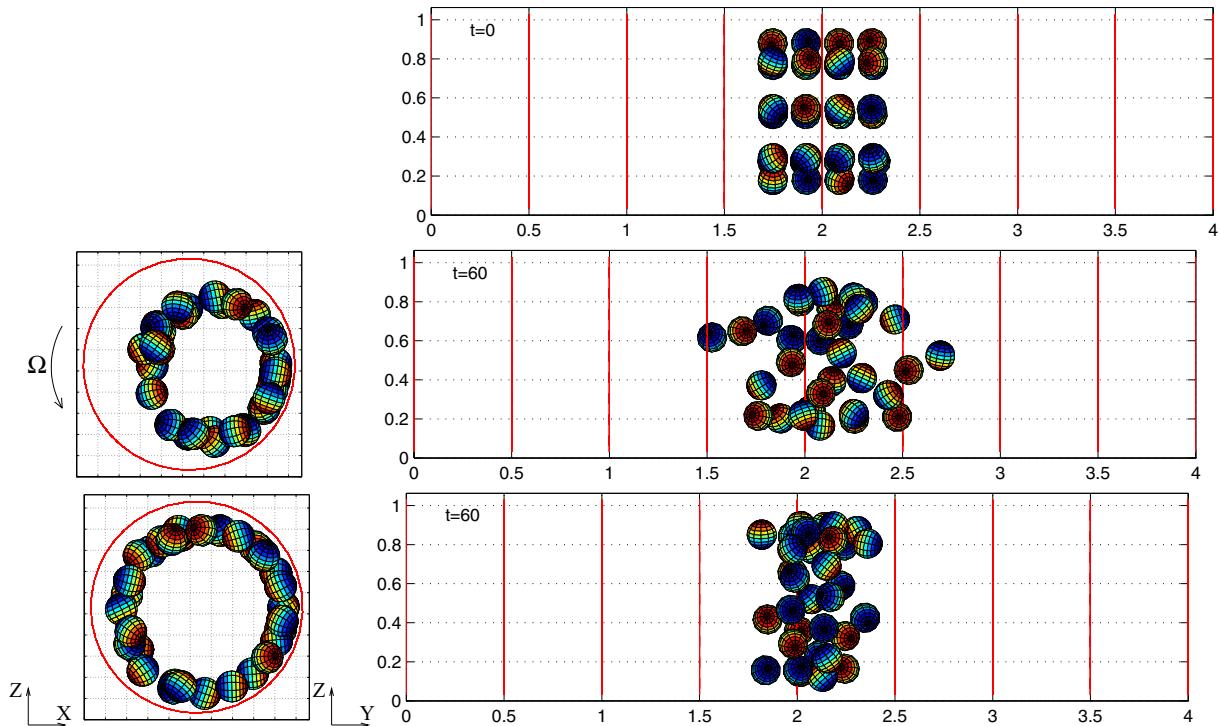


FIG. 5. (Color online) The side view (left) and the front view (right) of the initial position of 32 balls (top) and the position obtained at the angular speed $\Omega = 8$ (middle) and 12 (bottom) rad/sec at $t = 60$ sec.

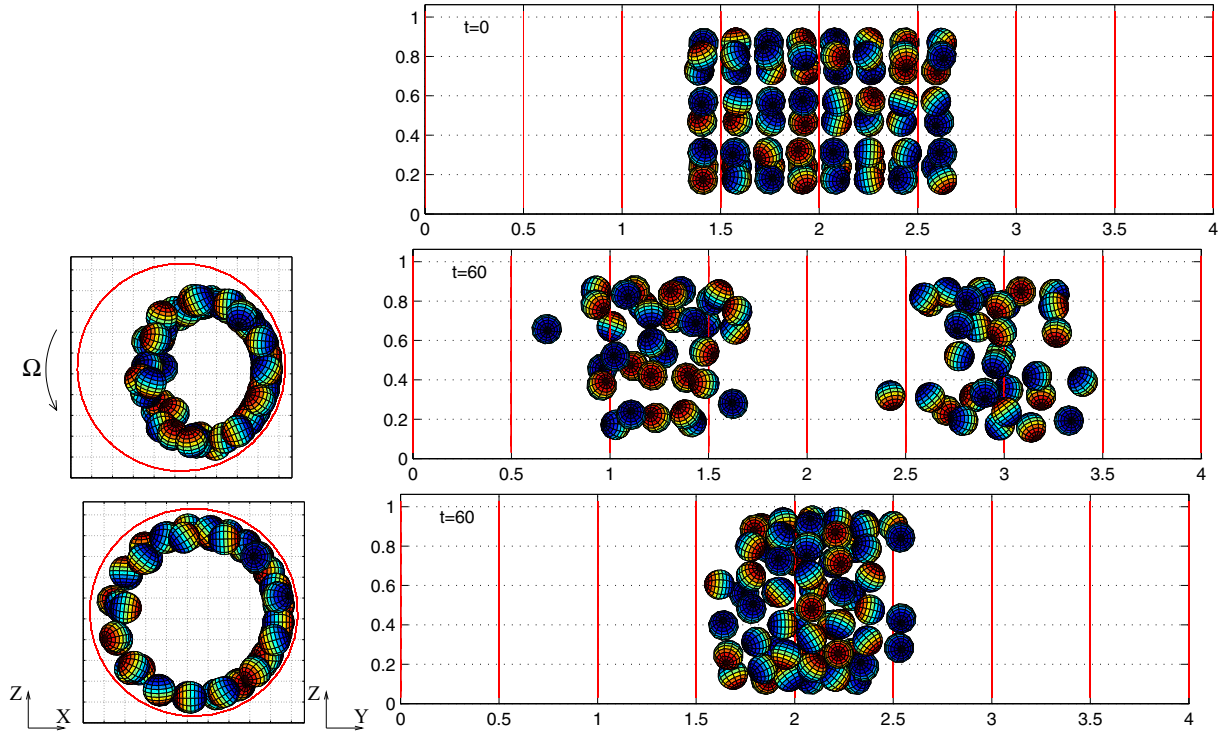


FIG. 6. (Color online) The side view (left) and the front view (right) of the initial position of 64 balls (top) and the position obtained at the angular speed $\Omega = 8$ (middle) and 12 (bottom) rad/sec at $t = 60$ sec.

respectively. The threshold for forming a circular band is about 30 balls for the conditions considered in this paper. The particle Reynolds numbers $Re_p = 2aU_p/\nu$ based on the average speed U_p of particles are about 2.28 and 4.28, respectively, for the angular speed Ω equal to 8 and 12 rad/sec.

Observing the trajectories of 32 balls in Fig. 8, we have found that the balls aggregate when the balls move from the front ($x = 1$) to the back ($x = 0$) through the upper portion of the cylinder and then they separate (spreading out in the direction of the cylinder axis) when the balls move from the back to the front through the lower portion of the cylinder. To analyze the aggregation and separation of the particles, we define the speed as $V_r = \sqrt{V_1^2 + V_3^2}$ in the xz plane from the particle translation velocity $\mathbf{V} = (V_1, V_2, V_3)$. The speed V_r tells us how fast each particle moves in the plane perpendicular to the cylinder axis directions, especially how it moves within a cluster when it is part of such a cluster. When each particle moves up from the front of the cylinder to the top of the cylinder, the speed in the x direction, $|V_1|$, is increasing by the rotation and the one in the z direction, $|V_3|$, is suppressed by the rotation and the gravity. Once it passes the top position and moves into the back portion of the cylinder, the speed in the z direction is increasing dramatically since the rotation and the gravity work together; even the one in the x direction is decreasing to zero. This explains when the balls of a cluster move through the upper portion of the cylinder, their speeds V_r are increasing as shown in Fig. 9 (the left ones). When one ball enters the wake of another ball which is speeding up, it experiences reduced drag and drafts closer to the leading ball (e.g., see [22,23] for the drafting, kissing, and tumbling between two balls). Thus the group of balls with increasing speeds can aggregate due to the hydrodynamical interaction

between balls. For the part of a circular band formed by the balls moving from the back to the front through the lower portion of the cylinder, the balls separate and spread out due to the slowdown of the speed V_r (see Fig. 9). The slowdown is caused by the rotation when each ball moves from the back to the bottom of the cluster since the gravity cannot compete with the rotation. Once the ball starts moving up from the bottom to the front, the speed is suppressed further by the rotation and the counter effect of the gravity as in Fig. 9. Due to these effects of the speedup and slowdown, the particle speed V_2 in the cylinder central axis direction does not have a different sign as shown in Fig. 10. For those particles whose average mass centers are located to the right of the average mass center of all particles in the cylinder central axis direction, when they move from the front to the back through the upper (respectively, lower) portion of the cylinder, the speed V_2 is negative (respectively, positive). For those located to the left of the average mass center of all particles, the speeds V_2 are opposite to those located to the right. Hence the balls aggregate during the speedup of the speed V_r when the balls move from the front to the back through the upper portion of the cylinder and they separate because of the slowdown of the speed V_r when the balls move from the back to the front through the lower portion of the cylinder. Therefore the histories of the y coordinate of the particle mass centers in Figs. 7, 11, and 15 show oscillations in the y direction. To have a stabilized and compact circular band, a large enough number of balls and a fast angular speed are needed in order to balance both effects; e.g., the results of the 32 ball cases in Figs. 5 and 8 show that at the angular speed $\Omega = 8$ rad/sec, the particle speeds are just fast enough to have the aggregation which can overcome the separation. But at the angular speed $\Omega = 12$ rad/sec, the

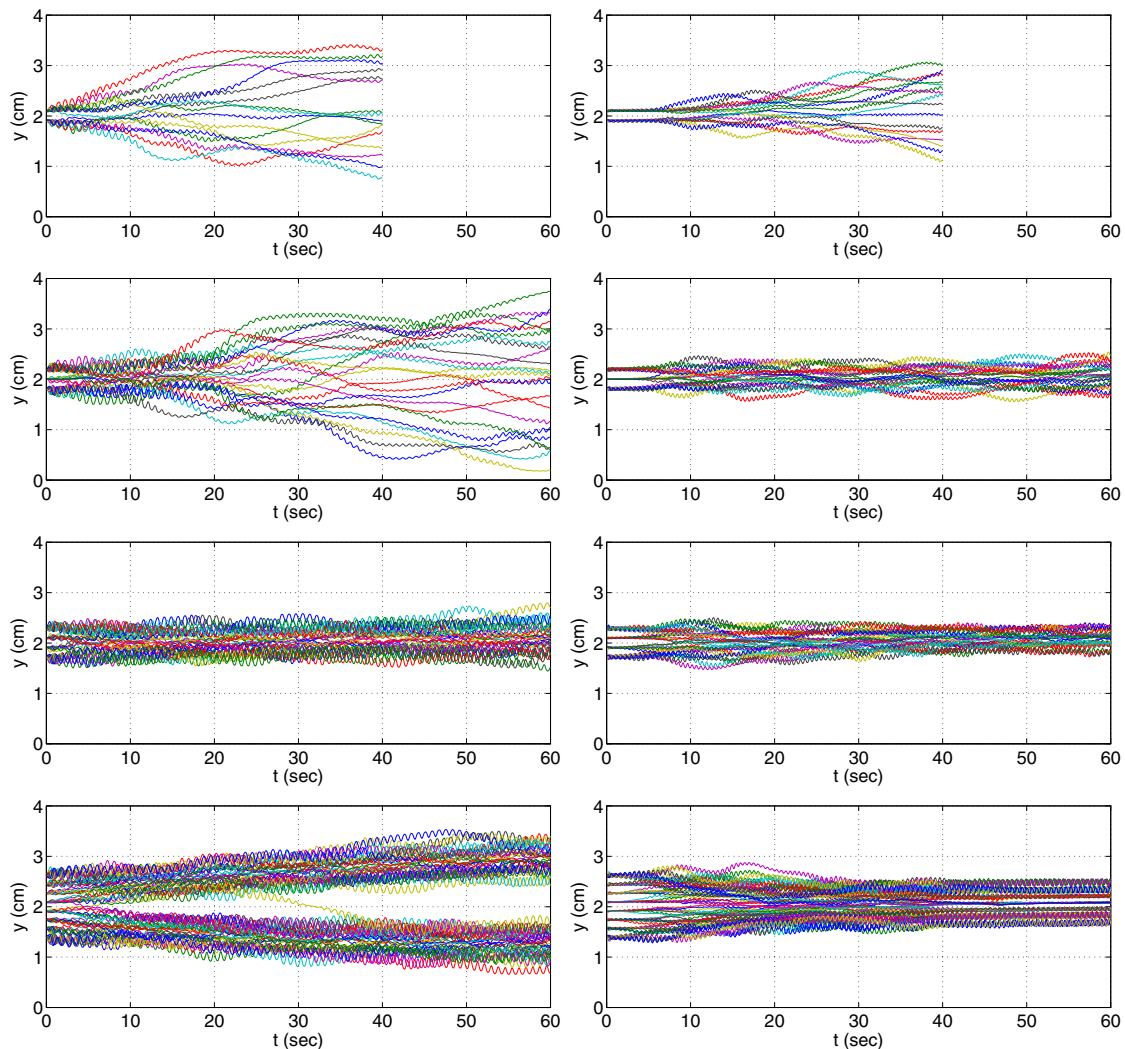


FIG. 7. (Color online) The histories of the y coordinate of the mass centers of 16, 24, 32, and 64 balls (from top to bottom) at $\Omega = 8$ (left) and 12 (right) rad/sec.

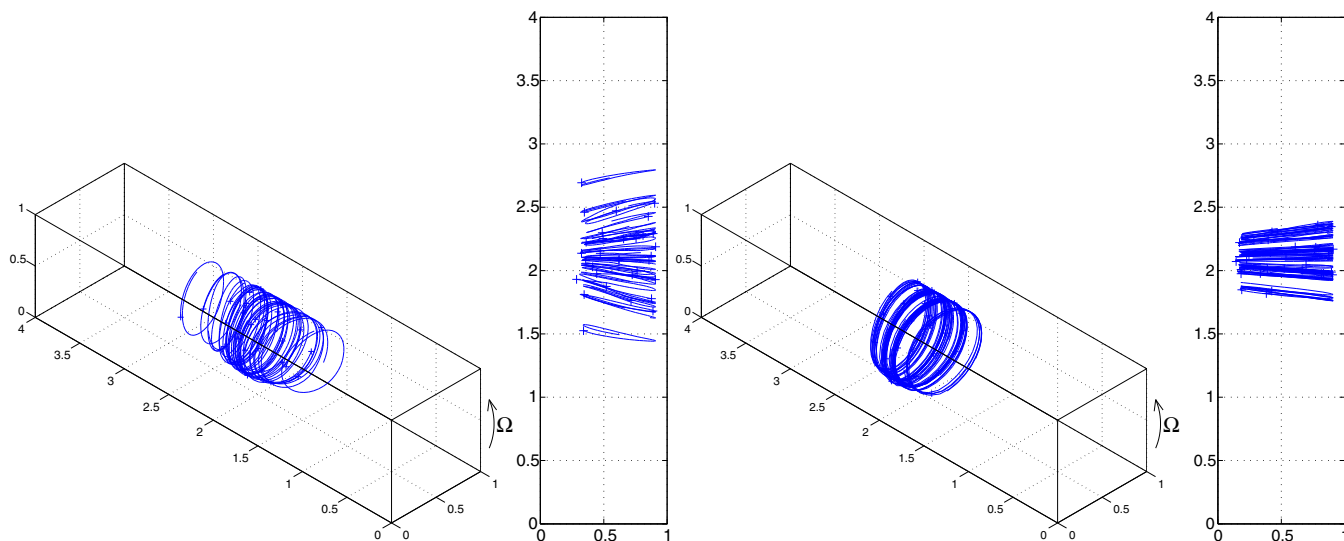


FIG. 8. (Color online) The trajectories and the top view of the trajectories of 32 balls at the angular speed $\Omega = 8$ (left two) and 12 (right two) rad/sec for $59 \leq t \leq 60$ sec. The unit is cm.

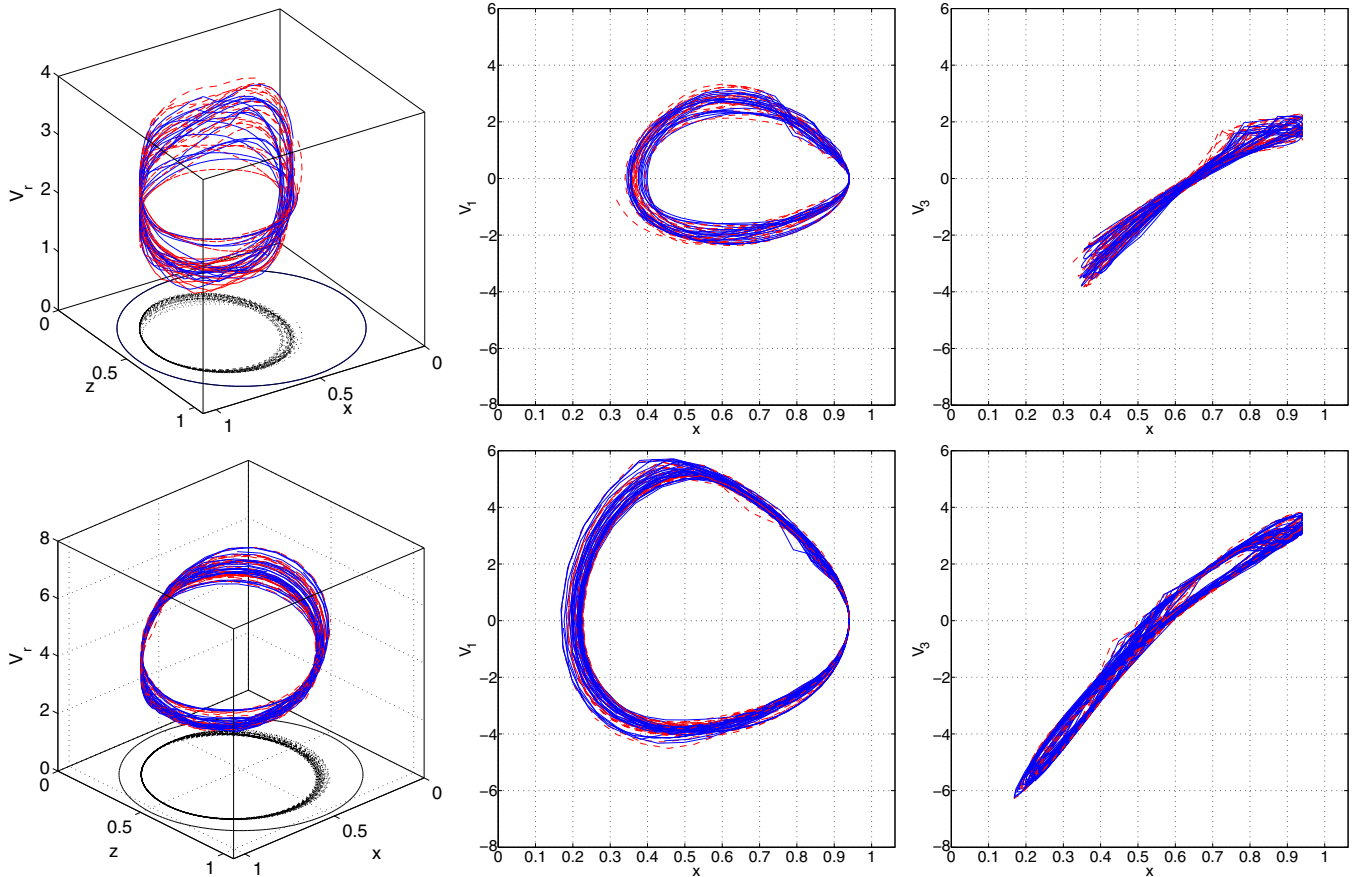


FIG. 9. (Color online) The speed $V_r = \sqrt{V_1^2 + V_3^2}$ (left) of particles in the xz plane vs the particle's x and z coordinates, V_1 (middle) and V_3 (right) for the cases of $\Omega = 8$ (top), and 12 (bottom) rad/sec for $59 \leq t \leq 60$ sec. The blue solid (respectively, red dashed) lines are associated with the particles whose average mass centers are located to the right (respectively, left) of the average mass center of all particles in the cylinder axis direction. The black dotted lines (in the left figure) are the projected particle trajectories in the xz plane and the black line in the xz plane is the boundary of the cylinder.

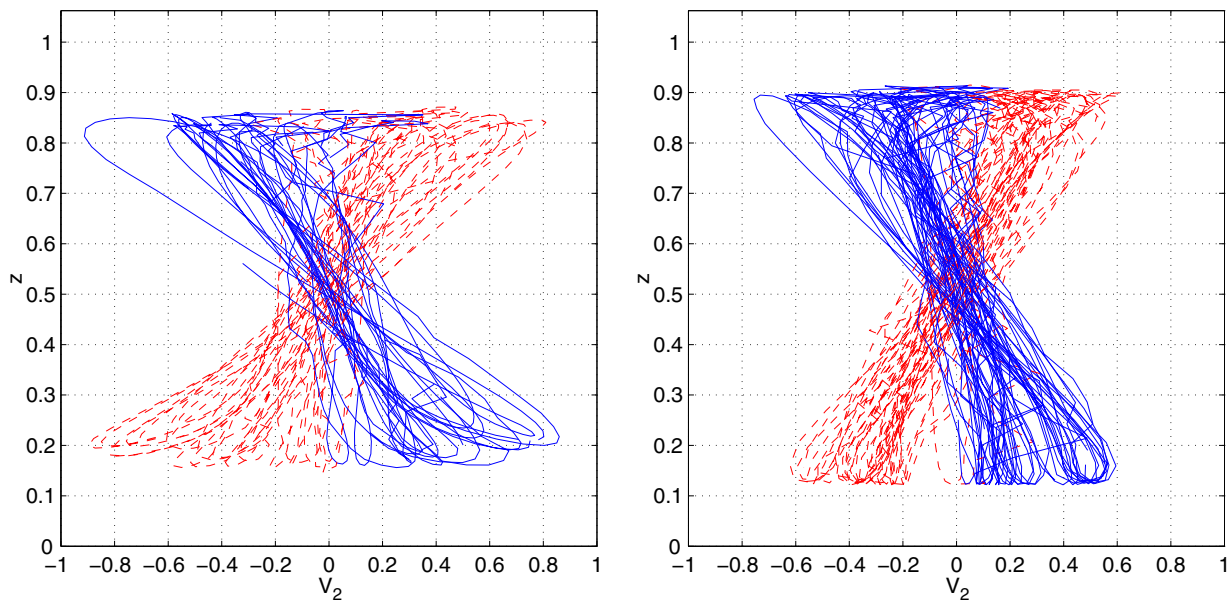


FIG. 10. (Color online) The particle speed V_2 in the cylinder central axis direction vs the particle z coordinate for the cases of $\Omega = 8$ (left) and 12 (right) rad/sec for $59 \leq t \leq 60$ sec. The blue solid (respectively, red dashed) lines are associated with the particles whose average mass centers are located to the right (respectively, left) of the average mass center of all particles in the cylinder axis direction.

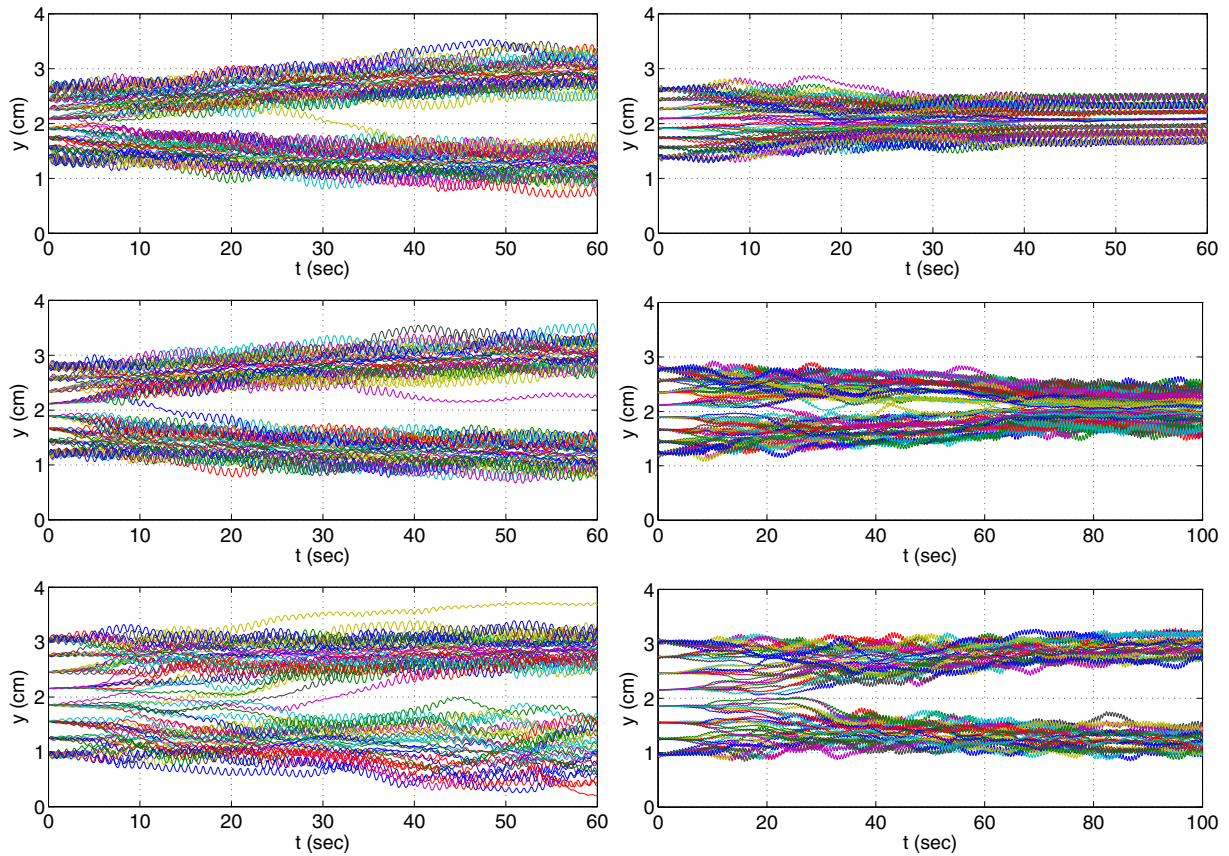


FIG. 11. (Color online) The histories of the y coordinate of the mass centers of 64 balls with initial gap sizes $a/4$, a , and $2a$ (from top to bottom): $\Omega = 8$ (left) and 12 (right) rad/sec.

particle interaction is stronger so that a compact circular band is formed. Similarly for the 64 ball case at lower angular speed $\Omega = 8$ rad/sec in Figs. 6 and 7, the balls spread out a little bit and segregate into two loose circular bands; but at $\Omega = 12$ rad/sec the particle interaction can pull all 64 balls together

in one compact circular band. Thus the particle segregation also depends on the relative motion between the particles and rotating flow field. Actually the distance between particles does matter concerning the formation of the circular bands. In Fig. 11, the histories of the y coordinate of the particle mass

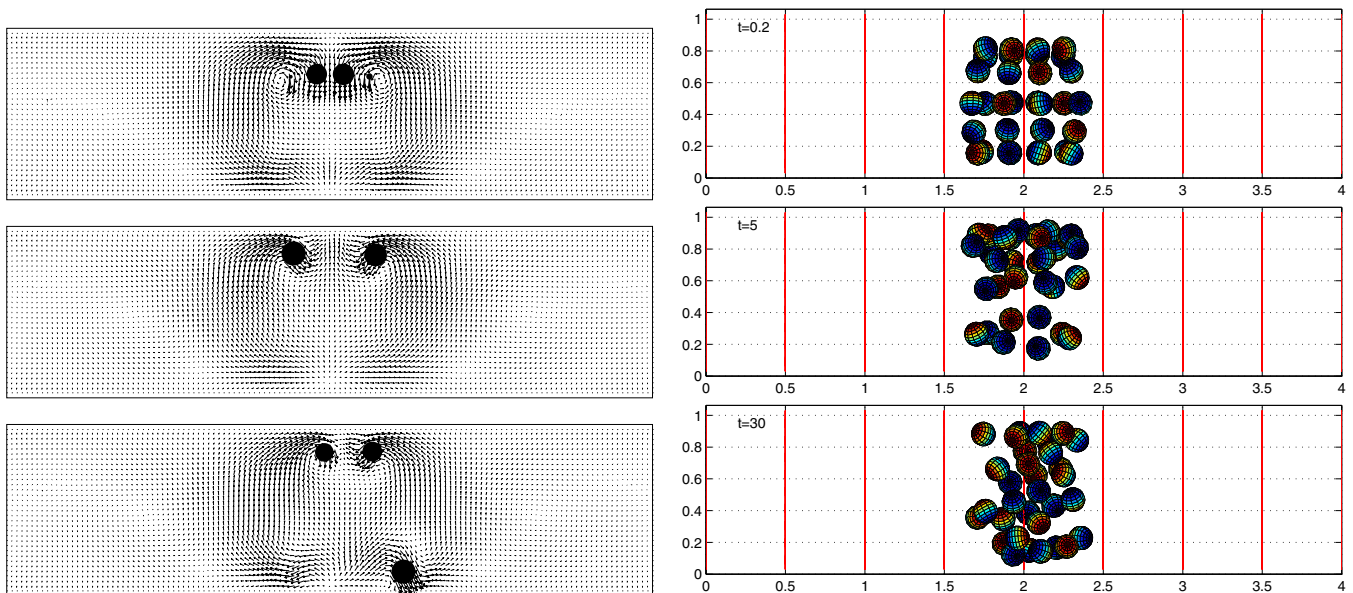


FIG. 12. (Color online) The projection of the velocity field on the vertical plane passing through the central axis of the cylinder for the case of 32 balls (left) and the front view of the position of 32 balls (right) at $t = 0.2, 5$, and 30 sec (from top to bottom) with $\Omega = 12$ rad/sec.

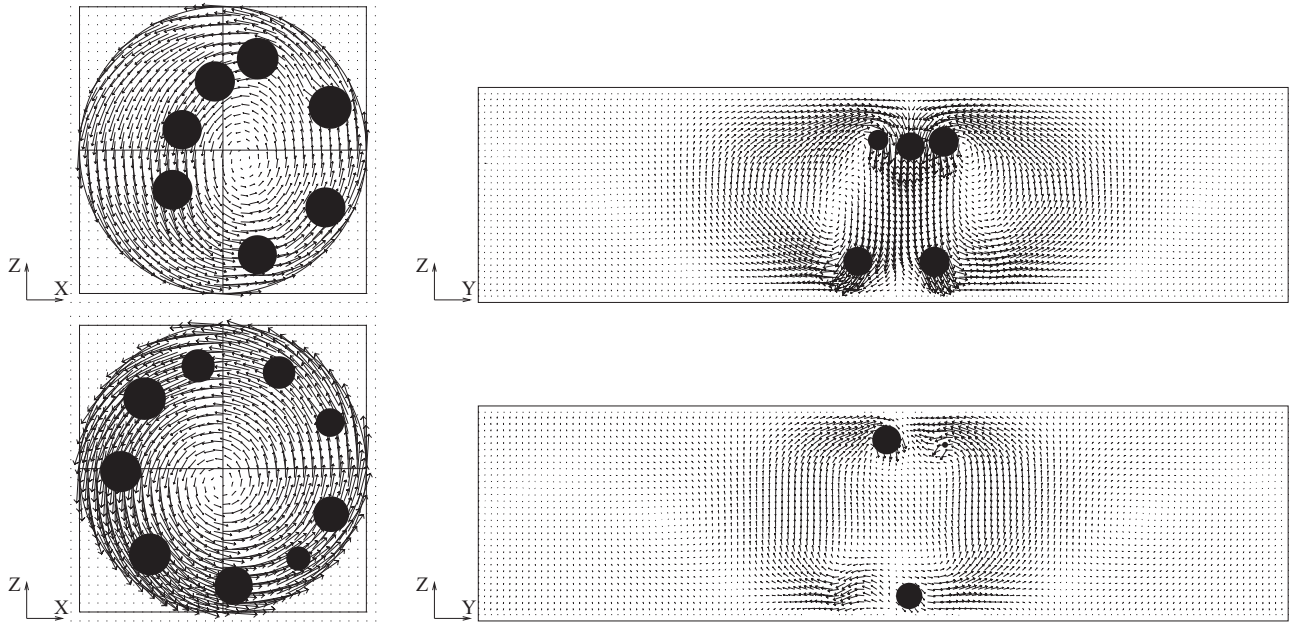


FIG. 13. The projection of the velocity field on the vertical plane at the middle of the circular band (left) and the vertical plane passing through the central axis of the cylinder (right) for the case of 32 balls at $t = 60$ sec: $\Omega = 8$ (top) and 12 (bottom) rad/sec.

centers are shown for different values of the initial gap size d_g . The particle interaction at $\Omega = 8$ rad/sec cannot pull all 64 balls into one circular band. The balls split into two groups for all three initial gap sizes and form circular bands except for one group of the balls for the case of $d_g = 2a$. At the angular speed

$\Omega = 12$ rad/sec, the threshold of the initial gap size for forming a circular band is $d_g = a$. There are two circular bands formed for the 64 balls with $d_g = 2a$, but the 64 balls with the initial gap size $d_g = a$ interact and finally come together to form a circular band at $t = 60$ sec as in Fig. 11. The formation of a

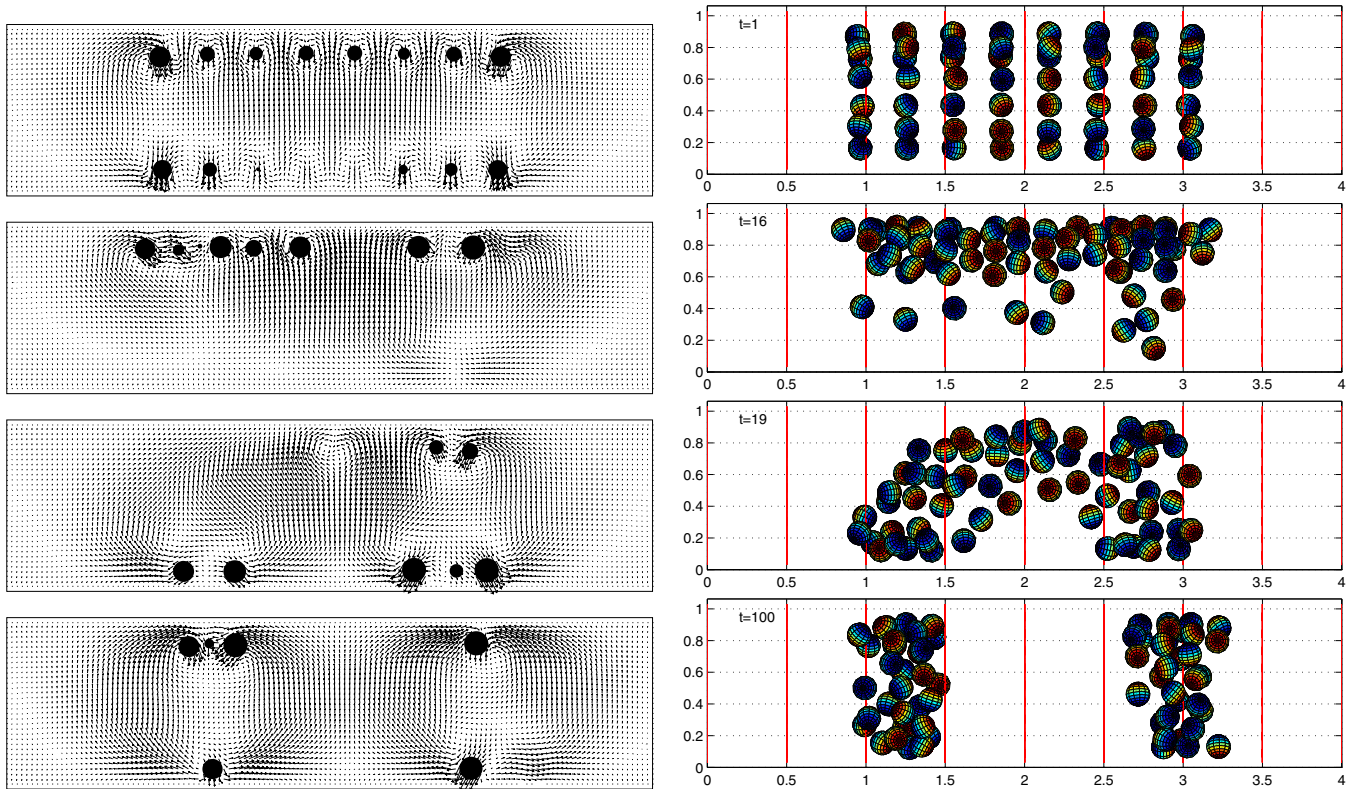


FIG. 14. (Color online) The projection of the velocity field on the vertical plane passing through the central axis of the cylinder for the case of 64 balls (left) and the front view of the position of 64 balls (right) at $t = 1, 16, 19,$ and 100 sec (from top to bottom) with $\Omega = 12$ rad/sec and the initial gap size $d_g = 2a$.

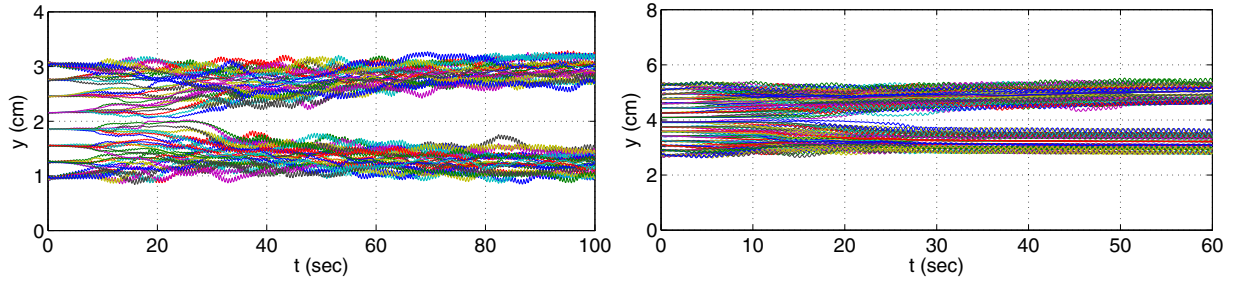


FIG. 15. (Color online) The histories of the y coordinate of the mass centers of 64 balls with the initial gap size $d_g = 2a$ (left) and 128 balls with the initial gap size $d_g = a/4$ (right).

circular band of the 64 balls with the initial gap size $d_g = a$ is much slower than the one with $d_g = a/4$ at $\Omega = 12$ rad/sec. These results show that the particle interaction has a short range effect on the formation of circular bands.

B. Effect of the band formation on the fluid flow field

Even the Reynolds numbers and Ekman numbers are in a different regime for the cases considered in this paper; we have obtained the circular bands like those in [10]. In experiments, it is not easy to set up the initial positions of the particles

like those chosen in direct numerical simulations, but those initial positions help us to understand the formation of circular bands and the development of the flow field inside the cylinder. For the case of 32 balls at $\Omega = 12$ rad/sec studied in the previous subsection, the projections of the velocity field on the vertical plane passing through the central axis of the cylinder at different time are shown in Fig. 12. The circulation of the velocity field is created by the particle motion and concentrated in the middle portion of the cylinder. To show why the velocity field at the middle of the cluster is slightly different from those observed in [10], we have shown the cross sections of the

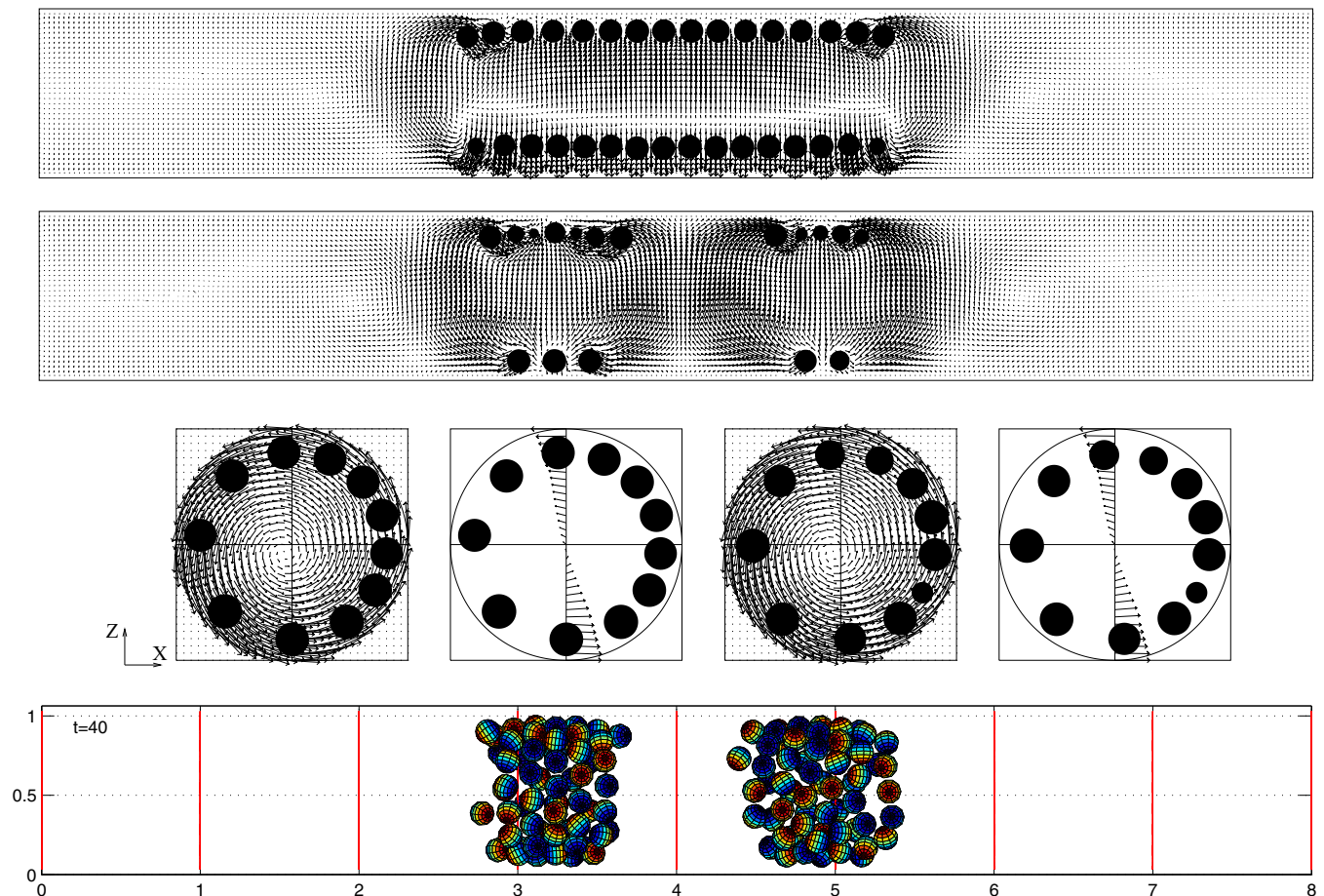


FIG. 16. (Color online) The projection of the velocity field on the vertical plane passing through the central axis of the cylinder for the case of 128 balls at $t = 0.4$ (top) and 40 sec (middle), those on the plane at the middle of the cluster at $y = 3.21875$ and the one on the vertical line through the cylinder center axis (left two in the middle) and $y = 5$ and the one on the vertical line through the cylinder center axis (right two in the middle) at $t = 40$ sec, and the front view of the position of 128 balls (bottom) at $t = 40$ sec.

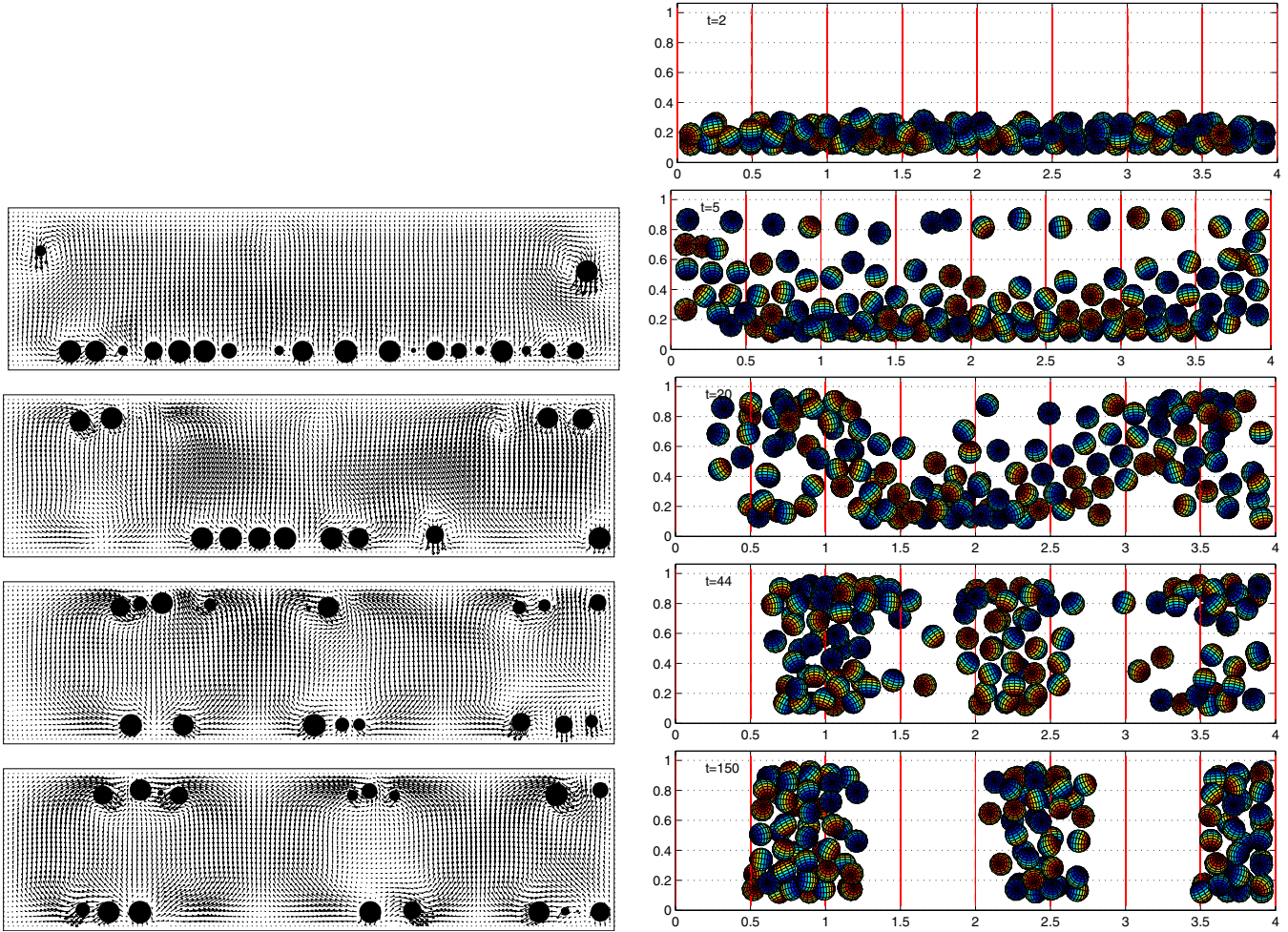


FIG. 17. (Color online) The projection of the velocity field on the vertical plane passing through the central axis of the cylinder for the case of 128 balls (left) and the front view of the position of 128 balls (right) at $t = 2, 5, 20, 44,$ and 150 sec (from top to bottom) with $\Omega = 12$ rad/sec.

flow field at the middle of circular band of 32 balls and the projection of the velocity field on the vertical plane passing through the cylinder central axis of the cylinder in Fig. 13. For the case of $\Omega = 8$ rad/sec, due to the rotating center of flow field (the left top figure in Fig. 13) located to the right of the cylinder central axis, the velocity projected on the vertical plane through the cylinder central axis points downward at the center of the cluster, which is same as the one in [10]. But for the other case of $\Omega = 12$ rad/sec, the rotating center of flow field (the left bottom panel in Fig. 13) is almost under the cylinder central axis so that the velocity on the vertical plan through the cylinder central axis does not point downward at the center of the cluster as in [10]. The distances of the rotating center to the cylinder central axis are $\Delta R = 0.073$ and 0.058 cm for $\Omega = 8$ and 12 rad/sec, respectively. Then the Rossby numbers $Ro = U/\Omega R$, where $U = \Omega \Delta R$ is the relative velocity of the secondary flow associated with the bands as considered in [6], are 0.146 and 0.116 . For both angular speeds, the Rossby numbers are not small and the inertial effect cannot be ignored as in [10].

For the evolution of the flow field related to two circular bands, the results of the case of 64 balls with the initial gap size $d_g = 2a$ and the angular speed $\Omega = 12$ rad/sec are shown in Figs. 14 and 15. We have observed no specific pattern

concerning the flow field from the beginning as in Fig. 14. The particles break into two circular bands between $t = 16$ and 19 sec and then two bands move away from each other as in Fig. 15. The projected velocity fields at $t = 19$ and 100 sec in Fig. 14 show that the two circulations move away from each other. The projected velocity field at $t = 100$ sec. in Fig. 14 is similar to the one obtained experimentally in [10], but the development of the flow field shows that the circulation of the flow field is caused by the motion of the particles in the two circular particle bands and there are no secondary flows occurring and helping the formation of the circular bands. For the case of 128 balls in a truncated cylinder of length $L = 8$ cm at the angular speed $\Omega = 12$ rad/sec with the initial gap size $d_g = a/4$, the particles are initially placed on 16 circles in the middle of the cylinder as in the previous subsection. Later they break into two compact circular bands as shown in Figs. 15 and 16. There are 63 and 65 particles in these two circular bands, respectively, which are consistent with the results of the 64 particles at the angular speed $\Omega = 12$ rad/sec discussed in the previous subsection. The figure of the circulation of the flow field at $t = 0.4$ sec in Fig. 16 clearly shows that there is only one large circulation. Two small circulations next to the large one at $t = 0.4$ sec

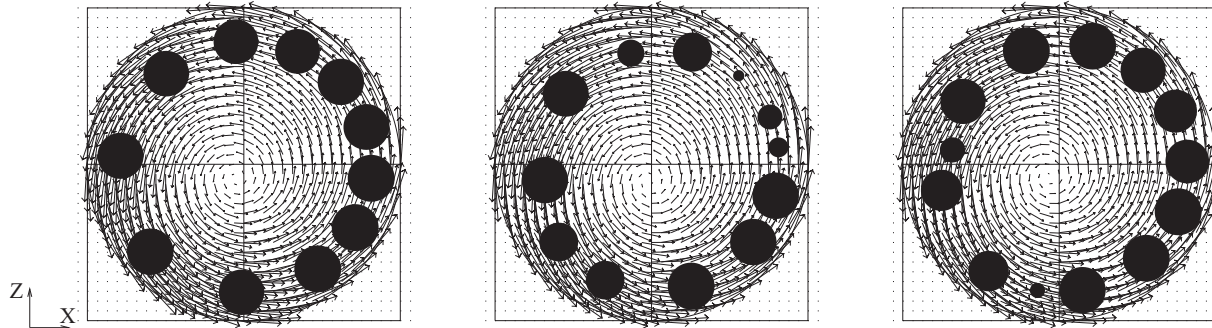


FIG. 18. The projection of the velocity field on the vertical plane at the middle of each circular bands for the case of 128 balls at $t = 150$ seconds: $y = 0.875, 2.5,$ and 3.75 cm (from left to right).

are created by the strong advection due to the particle motion and stay there all the time even when the balls split into two clusters as the one at $t = 40$ sec. These secondary flows are very weak for both cases. For both clusters in Fig. 16, the cross sections of the flow field at the middle of the circular band show that the rotating centers are located to the left of the cylinder central axis. Thus the velocity projected on the vertical plan through the cylinder central axis points upward at the center of the cluster as shown in the middle of Fig. 16.

To have the circular bands like the one in Fig. 2, we have considered the case of 128 balls in a truncated cylinder of length $L = 4$ cm. We have first placed 128 balls on 16 circles in the middle of the cylinder with the initial gap size $d_g = a/4$ as in the previous subsection and then let them settle at the zero angular speed. The balls settle down at the bottom of the cylinder after 2 sec as shown in Fig. 17. Then the cylinder rotates at the angular speed $\Omega = 12$ rad/sec. The 128 balls first move up and down inside the rotating cylinder and interact with the fluid. At $t = 5$ sec, there is no specific flow field pattern in the cylinder. About $t = 20$ sec, two outer bands next to the two ends of the cylinder start forming. Gradually three circular bands, which are similar to the one obtained experimentally in Fig. 2, are formed as shown in Fig. 17. The wavelength between two left bands at $t = 150$ sec is $3.25R$ and the distance from the leftmost band to the left end of the cylinder is also about half of the above wavelength. The right circular band has been pushed to the right end of the cylinder with no room to move. The wavelength is in good agreement with the wavelengths obtained in [10], which are between $3.2R$ and $3.3R$, for the case of $L/R = 8$. The cross sections of the flow field at the middle of each circular bands ($y = 0.875, 2.5,$ and 3.75 cm) are shown in Fig. 18. We observe that the rotating centers of flow field of each cross section are located either to the left of the cylinder central axis or right under the cylinder central axis. Thus the velocity projected on the vertical plan through the cylinder central axis points either upward or other directions at the center of the cluster as shown in the lower left one in Fig. 17. The distances of the rotating center to the cylinder central axis are $\Delta R = 0.0572, 0.0473,$ and 0.0481 cm, respectively, for $y = 0.875, 2.5,$ and 3.75 cm. The

Rossby numbers $Ro = U/\Omega R$ are 0.1144, 0.0946, and 0.0962, respectively, for $y = 0.875, 2.5,$ and 3.75 cm. The Ekman number for this case is 0.05 as discussed at the beginning of Sec. III A. Since both the Ekman number and the Rossby number are not too small, the inertial effect and diffusion cannot be ignored for the perturbation analysis.

IV. CONCLUSION

In this paper we have applied a distributed Lagrange multiplier fictitious domain method with a finite element method and operator splitting to simulate rotating suspension of particles and to study the interaction between balls and fluid in a fully filled and horizontally rotating cylinder. The formation of circular bands studied in this paper is mainly caused by the interaction between particles themselves. Within a circular band, the part of the band formed by the particles moving from the front to the back through the upper portion of the cylinder becomes more compact due to the particle interaction strengthened by the speedup of the particle speeds first by the rotation and later by the rotation and the gravity. The part of a band formed by the particles moving from the back to the front through the lower portion of the cylinder is always loosening up and spreading out due to the slowdown of the particle motion first by the rotation and later by the rotation and the counter effect of the gravity. To have a compact circular band, particles have to interact among themselves continuously through the entire circular band at an angular speed so that the separation of particles can be balanced by their aggregation. Hence the balance of the gravity, the angular speed, and the fluid flow inertia and the number of particles are important to the formation of circular bands.

ACKNOWLEDGMENTS

The authors acknowledge the valuable comments and suggestions of J. J. Feng, H. H. Hu, and P. Tong. T.W.P. and R.G. acknowledge the support of NSF (Grant No. DMS-0914788).

[1] M. Tirumkudulu, A. Tripathi, and A. Acrivos, *Phys. Fluids* **11**, S13 (1999).

[2] M. Tirumkudulu, A. Mileo, and A. Acrivos, *Phys. Fluids* **12**, 1615 (2000).

- [3] D. D. Joseph, J. Wang, R. Bai, B. H. Yang, and H. H. Hu, *J. Fluid Mech.* **496**, 139 (2003).
- [4] W. R. Matson, B. J. Ackerson, and P. Tong, *Phys. Rev. E* **67**, 050301 (2003).
- [5] W. R. Matson, M. Kalyankar, B. J. Ackerson, and P. Tong, *Phys. Rev. E* **71**, 031401 (2005).
- [6] W. R. Matson, B. J. Ackerson, and P. Tong, *J. Fluid Mech.* **597**, 233 (2008).
- [7] A. P. J. Breu, C. A. Kruelle, and I. Rehberg, *Europhys. Lett.* **62**, 491 (2003).
- [8] S. G. Lipson, *J. Phys.: Condens. Matter* **13**, 5001 (2001).
- [9] S. G. Lipson and G. Seiden, *Physica A* **314**, 272 (2002).
- [10] G. Seiden, M. Ungarish, and S. G. Lipson, *Phys. Rev. E* **72**, 021407 (2005).
- [11] G. Seiden and P. J. Thomas, *Rev. Mod. Phys.* **83**, 1323 (2011).
- [12] J. H. Lee and A. J. C. Ladd, *Phys. Rev. Lett.* **95**, 048001 (2005).
- [13] J. H. Lee and A. J. C. Ladd, *J. Fluid Mech.* **577**, 183 (2007).
- [14] G. Seiden, M. Ungarish, and S. G. Lipson, *Phys. Rev. E* **76**, 026221 (2007).
- [15] R. Glowinski, T.-W. Pan, T. Hesla, and D. D. Joseph, *Int. J. Multiphase Flow* **25**, 755 (1999).
- [16] R. Glowinski, T.-W. Pan, T. Hesla, D. D. Joseph, and J. Periaux, *J. Comput. Phys.* **169**, 363 (2001).
- [17] R. Glowinski, *Finite Element Methods for Incompressible Viscous Flow*, Handbook of Numerical Analysis Vol. IX, edited by P. G. Ciarlet and J. L. Lions (North-Holland, Amsterdam, 2003), pp. 3–1176.
- [18] T.-W. Pan, D. D. Joseph, R. Bai, R. Glowinski, and V. Sarin, *J. Fluid Mech.* **451**, 169 (2002).
- [19] B. H. Yang, J. Wang, D. D. Joseph, H. H. Hu, T.-W. Pan, and R. Glowinski, *J. Fluid Mech.* **540**, 109 (2005).
- [20] T.-W. Pan, R. Glowinski, and S. C. Hou, *Comput. Struct.* **85**, 955 (2007).
- [21] A. J. Chorin, T. J. R. Hughes, J. E. Marsden, and M. McCracken, *Commun. Pure Appl. Math.* **31**, 205 (1978).
- [22] J. Feng, H. H. Hu, and D. D. Joseph, *J. Fluid Mech.* **261**, 95 (1994).
- [23] D. D. Joseph, *Interrogations of Direct Numerical Simulation of Solid-Liquid Flows* (Springer, Berlin, 2002), <http://www.efluids.com/efluids/books/joseph.htm>.